

Evolution of LeTID defects in industrial multi-crystalline silicon wafers under laser illumination - Dependency of wafer position in brick and temperature

Zheng Yao ^{a,b,1}, Daqi Zhang ^{b,1}, Jian Wu ^b, Fangdan Jiang ^b, Guoqiang Xing ^b, Xiaodong Su ^{a,*}

^a School of Physical Science and Technology, and Jiangsu Key Laboratory of Thin Films, Soochow University, 1 Shizi Street, Suzhou, 215006, China

^b Canadian Solar Inc., 199 Lushan Road, SND, Suzhou, 215129, China



ARTICLE INFO

Keywords:

Light and elevated temperature-induced degradation
Multi-crystalline silicon brick
Injection dependent lifetime spectroscopy
Activation energy

ABSTRACT

In the past few years, a hot topic in both research and industrialization of p-type multi-crystalline silicon (mc-Si) solar cells is to investigate the mechanism, measurement and mitigation of the light- and elevated temperature-induced degradation (LeTID), which has been found to be a bulk-sensitive degradation behavior and is dependent on the degradation condition. In this paper, we study the influence of silicon bulk property on LeTID from five representative positions along a relative low resistivity ($0.82\text{--}1.33 \Omega \text{ cm}$) p-type mc-Si brick. The evolution of degradation and regeneration under different laser illumination conditions are investigated. Identical defect capture cross section ratio k values of ~ 35 at mid-gap along the brick height are found. For the first time, the activation energy for degradation ($E_{a,\text{deg}}$) and regeneration ($E_{a,\text{reg}}$) along the brick are studied, which shows E_a , $\text{deg} = E_{a,\text{reg}}$ and a tendency of larger values towards the brick bottom. These results indicate that the LeTID in the whole brick might be induced by a single defect and thus mitigated in a single manner. **Besides, a laser illumination of 45 kW/m^2 at 142°C for 100 s is able to induce over 90% degradation for all wafers, which could be used as a universal and fast LeTID test condition.**

1. Introduction

High efficiency multi-crystalline silicon (mc-Si) solar cells with the passivated emitter and rear cell (PERC) technology have been commercialized in the past years [1]. One critical issue of the PERC cells is the efficiency degradation under illumination, among which the light- and elevated temperature-induced degradation (LeTID) has been shown to cause $>10\%$ degradation [2]. Although the root cause of LeTID is still not well understood yet, studies revealed it could be bulk-related and dependent on the degradation conditions [3–6]. Besides, LeTID is observed not only in p-type mc-Si, but also in p-type Czochralski (Cz) [7] and Float-Zone (Fz) Si [8], and even in n-type Si [9]. Moreover, LeTID is strongly related to previous thermal processes, such as firing [10,11], dark annealing [12,13], which may release hydrogen from hydrogen-rich dielectric layers and modulate the hydrogen charge state to become a precursor of recombination-active defect. Based on these facts, the involvement of excess hydrogen in the bulk is suggested as part of the root cause of LeTID [14]. Some behavior of LeTID both in the dark

and under illumination might be explained by the migration of and interactions between charged hydrogen species and dopant atoms within the diffused layers and the silicon bulk [15].

In the case of p-type mc-Si, the ingots/bricks vary in dopants, contaminants [16], grain sizes, and crystallographic defects [17] regarding to different positions. However, the influence of material properties on LeTID is rarely reported, especially for the relatively low resistivity wafers. Chung et al. showed that the degradation rate of LeTID during laser illumination is not majorly influenced by the wafer's position within the brick of resistivity ranging from 1.6 to $2.2 \Omega \text{ cm}$ [18]. Kersten et al. found that the top brick cells showed a slower degradation rate and a lower degradation level among the whole brick [19]. The major difference of the two work is the degradation condition: Kersten et al. used current injection (V_{oc} mode, close to 1 kW/m^2) at 75°C , while Chung et al. used a laser illumination (irradiance of 34.6 kW/m^2) at 140°C . Although some equivalency between the current injection and light soaking, by halogen lamps or laser illumination, has been demonstrated [20], the difference in wafer properties along the brick height can still

* Corresponding author.

E-mail address: xdsu@suda.edu.cn (X. Su).

¹ Correspondence These authors contributed equally to this work and should be considered co-first authors.

lead to different degradation behavior.

In this study, we investigate the temperature dependence as well as the evolution of lifetime degradation and regeneration under laser illumination of wafers from five different positions along a p-type mc-Si brick. The brick resistivity is relatively low which is rarely studied before [21,22]. The injection dependent lifetime spectroscopy (IDLS) are used to determine the defect capture cross section ratio (k), and temperature-dependent rates are used to calculate the activation energy (E_a) of the involved defects. It was confirmed that k values along the brick height are identical, and the activation energy for degradation ($E_{a,\text{deg}}$) shows no difference with the activation energy for regeneration ($E_{a,\text{reg}}$) in the same wafer position. Finally, we propose a universal and fast LeTID test condition for the whole brick wafers.

2. Experimental details

In this experiment, symmetric lifetime test structures were made on the full size $157 \times 157 \text{ mm}^2$ wafers ($180 \mu\text{m}$) with resistivity ranging $0.82\text{--}1.33 \Omega \cdot \text{cm}$, which were cut from a p-type mc-Si brick at five representative positions, as shown in Table 1. Fig. 1 shows photoluminescence (PL) images of the as-cut wafers to demonstrate the increasing grain size towards the top of the brick. Twenty sister wafers from each brick height were processed in an industrial PERC production line at Canadian Solar Inc. All wafers were double-side wet chemical textured, then double-side diffused in a POCl_3 tube furnace (S.C. New Energy Technology, China) with a sheet resistance of $135 \pm 10 \Omega/\square$. After the phosphosilicate glass (PSG) removal in HF, silicon nitride (SiN_x) layers with a thickness of $85 \pm 3 \text{ nm}$ and a refractive index of 2.08 ± 0.05 at 633 nm were deposited on both sides of the wafers using a plasma-enhanced chemical vapor deposition machine (S.C. New Energy Technology, China). The wafers were then fired at $790 \pm 4^\circ\text{C}$ (actual peak temperature) in a commercial infrared fast-firing furnace (Folungwin, China). The wafers underwent accelerated degradation and regeneration with a commercialized continuous wavelength laser at 45 kW/m^2 (DR laser, 950–980 nm, China) at different temperatures. A heating stage integrated with dry air cooling is used to control the wafer's temperature during laser illumination, and the wafer's temperature is measured by thermal couples connected to Keysight 34972 A. One full sized wafer from each position is used for each laser illumination condition. The effective minority carrier lifetime (τ_{eff}) were measured at wafer center *ex-situ* between each laser treatment intervals using a Sinton WCT-120 lifetime tester at room temperature. A Sinton WCT-120TS tool is used to acquire lifetime data at elevated temperature. The τ_{eff} values were extracted at an excess minority carrier density (Δn) equal to 10% of doping concentration (N_A). The lifetime distribution after firing is shown in Table 1, with maximum deviation less than $3 \mu\text{s}$. The normalized defect densities (NDD) are calculated using the equation below [23]:

$$\text{NDD}(t) = \frac{1}{\tau_{\text{laser}}(t)} - \frac{1}{\tau_{\text{fired}}} \quad (1)$$

where t , τ_{laser} , τ_{fired} is the laser treatment time, τ_{eff} of the sample after laser treatment, τ_{eff} of the sample after firing, respectively.

The fractional defect density (FDD) was calculated by Eq. (2) [24]:

$$\text{FDD}(t) = \frac{\text{NDD}(t)}{\text{NDD}_{\max}} \quad (2)$$

where NDD_{\max} is the maximum NDD extracted from the samples at the fully degraded state.

The recombination parameters such as the defect capture cross section ratio k and emitter saturation current ($J_{0,e}$), are obtained from IDLS data analysis by utilizing the fitting method D as proposed in Ref. [25].

3. The LeTID behavior under laser illumination

First, the impact of firing is studied to find out whether these low resistivity wafers show a typical LeTID behavior under the laser illumination condition. Fig. 2(a) compares the evolution of τ_{eff} with laser illumination times for the fired and unfired wafers from 5%-wafer illuminated with 45 kW/m^2 laser at 159°C . Distinguished degradation and regeneration are observed in the fired samples with maximum τ_{eff} degradation up to 37% relatively, while the unfired τ_{eff} keeps almost constant during laser illumination. Since the original τ_{eff} are different due to the hydrogen passivation of bulk defects during the firing, the calculated NDD are plotted in Fig. 2(b), confirming that the firing is the key to induce LeTID in these wafers. This result shows even for the state-of-the-art mc-Si wafers with overall metal impurity content $<30 \text{ ppbw}$, LeTID can still happen when the cell processing is not well controlled.

As the wafers in Fig. 2 are near the bottom of the brick, they contain the highest interstitial oxygen concentration (typical value of $4 \times 10^{15} \text{ cm}^{-3}$) along the brick. Previous study shows that the boron-oxygen (BO) defect formation and fully passivation take place within 100 s under 18 kW/m^2 at 150°C [26]. If the BO defect is the dominating factor of the degradation and regeneration processes in Fig. 2(a) and (b), little difference between unfired and fired wafers is expected and the unfired sample would show clear degradation and regeneration, which contradicts with the data. Therefore, we are confident to conclude that BO-LID does not play a dominant role in this work.

Fig. 2(c) shows the IDLS results during the laser illumination process of the fired wafers, in which the time-dependent lifetime varies mainly at low injection level. Furthermore, $J_{0,e}$ keeps as constant during the laser illumination in Fig. 2(d), which confirms that the lifetime variation is caused by the bulk Shockley-Read-Hall (SRH) recombination, rather than the surface passivation degradation. In Fig. 2(c), the IDLS spectrum almost recovers to the initial value at 600 s, similar to the reported LeTID behavior [27]. Fig. 2(d) shows the fitted k values (defect energy level assumed to be at mid-gap) remain nearly constant during the cycle, ranging from 31 to 37, in good accordance with the reported values for the LeTID defects [28].

We further explore the temperature-dependent FDD ($134\text{--}176^\circ\text{C}$) for different laser illumination durations (Fig. 3). At higher temperature, the FDD reaches the maximum more rapidly. For instance, only 6 s is required to reach maximum degradation at 176°C , while 85 s is required at 134°C .

4. Effect of wafer position and temperature

In this study, τ_{eff} evolution of wafers from the five positions are tested and k values are extracted at different laser illumination time. All wafers have almost the same k values lying within the errors shown in Fig. 4, indicating a uniform defect which causes the LeTID in all positions along the brick. The defect k value is 35 in average, similar to the recently reported k values for the LeTID defect, e.g. 26–36 by Morishige et al. [29], 27.7–37.7 by Fung et al. [14]. Since the same defect is responsible for the degradation for all wafers, the NDD value extracted at $0.1 N_A$ is proportional to the defect density and can be comparable for all the wafers (Appendix A for details).

Fig. 5 compares the temperature-dependent ($134\text{--}176^\circ\text{C}$) FDD-time evolution of the wafers from five positions, at a constant illumination

Table 1
Resistivity and τ_{fired} for the wafers.

wafer position (percent of height)	resistivity ($\Omega \cdot \text{cm}$)	$\tau_{\text{fired}} (\mu\text{s})$
95% (Top)	0.82	41 ± 1
65%	1.06	66 ± 1
45%	1.13	87 ± 3
25%	1.22	90 ± 2
5% (Bottom)	1.33	106 ± 1

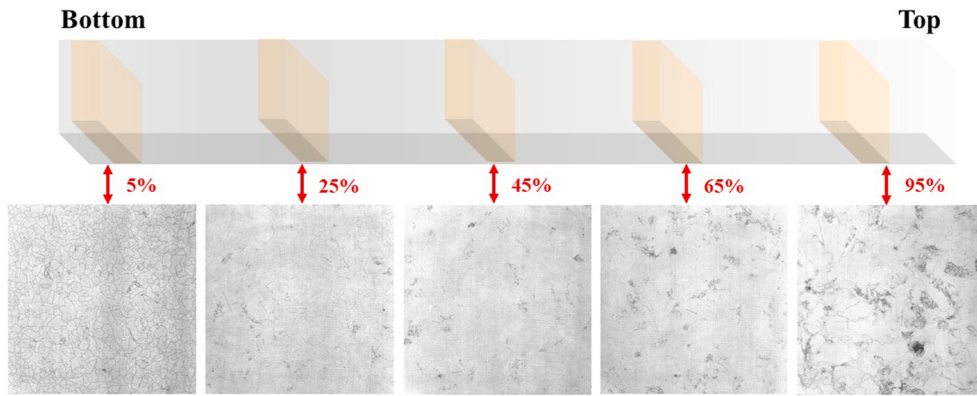


Fig. 1. Schematic of five representative positions in a brick ($157\text{ mm} \times 157\text{ mm} \times 680\text{ mm}$), and PL images of as-cut wafers sourced from relative positions in the ingot from the bottom of 5%, 25%, 45%, 65% and 95%, respectively.

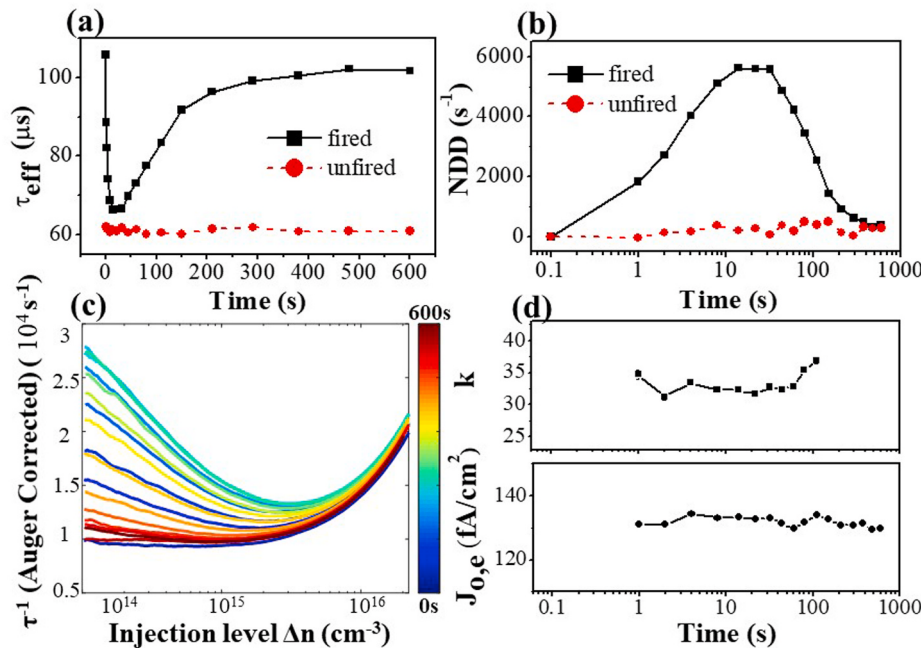


Fig. 2. Degradation and regeneration of 5%-wafers illuminated with 45 kW/m^2 laser at $159\text{ }^\circ\text{C}$ till 600 s : (a) Evolution of τ_{eff} for the fired (black solid line) and unfired (red dash line) wafers. (b) Evolution of NDD for the fired (black solid line) and unfired (red dash line) wafers. (c) IDLS curves for the fired wafers at different laser illumination time. (d) K value (upper panel) and $J_{0,e}$ (lower panel) variation by fitting the data in (c). The k values are given at mid-gap. (For interpretation of the references to color in this figure legend, the reader is referred to the Web version of this article.)

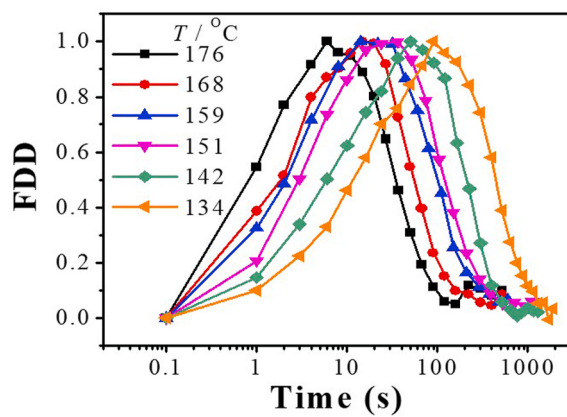


Fig. 3. FDD evolution of 5%-wafer at different temperatures under 45 kW/m^2 laser illumination.

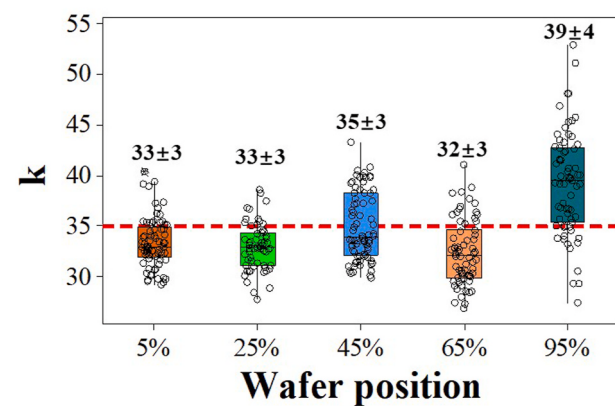


Fig. 4. Fitted k values for different wafers from the five positions.

intensity of 45 kW/m^2 . The wafers close to the brick bottom (e.g. 5%-wafer) show faster degradation and regeneration than those close to the brick top. This can be explained as its larger Δn at either room

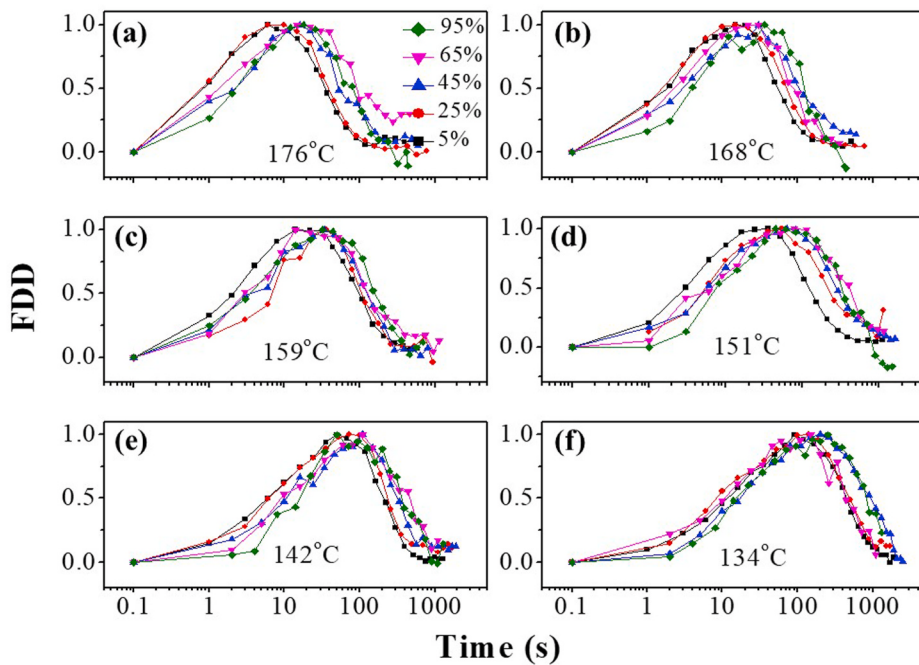


Fig. 5. FDD-time evolution of wafers at temperature of (a) 176 °C, (b) 168 °C, (c) 159 °C, (d) 151 °C, (e) 142 °C, and (f) 134 °C. The wafers from different positions are marked with different colors and symbols as indicated in (a). (For interpretation of the references to color in this figure legend, the reader is referred to the Web version of this article.)

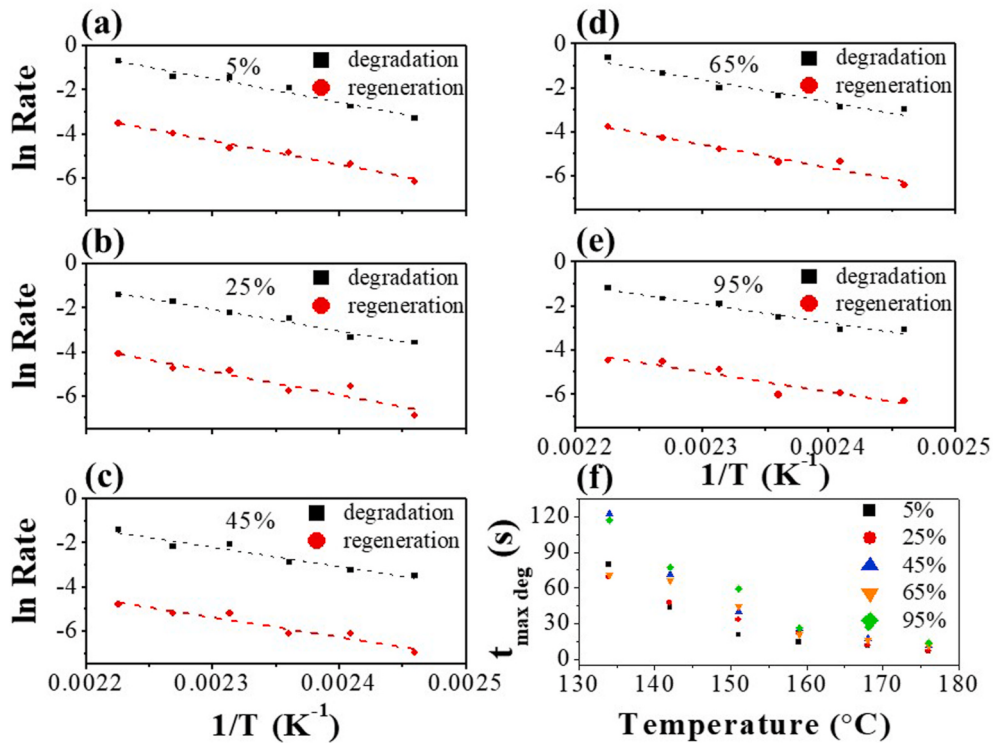


Fig. 6. Rate constants (in natural logarithm) of degradation (black squares) and regeneration (red dots) at different temperatures. (a) 5% brick height, (b) 25% brick height, (c) 45% brick height, (d) 65% brick height, (e) 95% brick height. The dash lines are linear fitting of the data. (For interpretation of the references to color in this figure legend, the reader is referred to the Web version of this article.)

temperature (Fig. 7) or 159 °C (Figure B, Appendix B). Moreover, we notice that for lower wafer temperature, the difference in FDD-time curves among wafers becomes less significant. For instance, the degradation for all wafers can reach more than 90% of their NDD_{max} at 142 °C within 100 s.

To quantitatively describe the degradation and regeneration process, the NDD-time curves are fitted with the following expression [27]:

$$\text{NDD}(t) = \text{NDD}_{\max} \{ [1 - \exp(-r_{\deg} t)] - (1 + A)[1 - \exp(-r_{\text{reg}} t)] \} \quad (5)$$

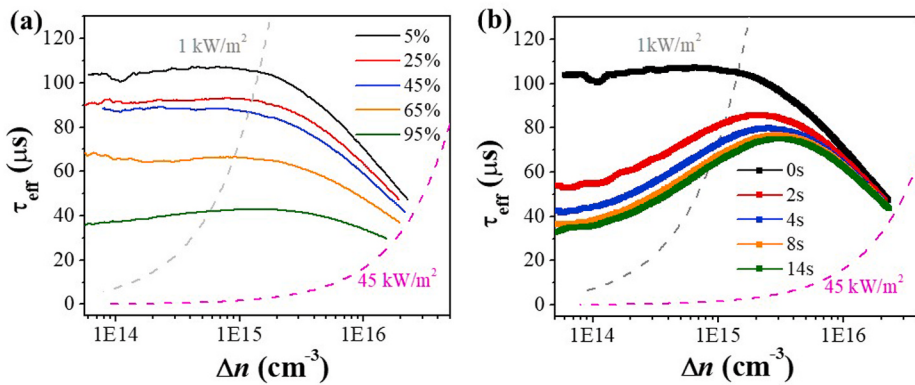


Fig. 7. (a) IDLS curves for the as-fired wafer of different brick height wafers@ room temperature, (b) IDLS curves during degradation for the 5%-wafer@ room temperature. The dashed lines represents the correlation between τ_{eff} and Δn at 1 kW/m^2 (gray dash line) and 45 kW/m^2 (magenta dash line) based on the quasi-steady-state photoconductance (QSSPC) method. The 1 kW/m^2 line is obtained from test data, while the 45 kW/m^2 line is calculated as 45 times of 1 kW/m^2 .

where NDD_{max} is the maximum possible NDD, A is a factor to account for improvement in effective lifetime (compared to the initial state) with values ranging from -0.2 to 0.2 , r_{deg} and r_{reg} are the degradation and regenerations rates, respectively. The rates shown in Fig. 6 are considered as constants due to the nearly constant injection level under high intensity illumination condition, which will be discussed in the next section. By fitting the dependence of r_{deg} and r_{reg} on temperature with Arrhenius equation [30], we got the values of degradation activation energy ($E_{\text{a,deg}}$) and regeneration activation energy ($E_{\text{a,reg}}$) for each wafer in Table 2. The Arrhenius function was defined as

$$r_{\text{deg/reg}} = C \times \left[-\frac{E_{\text{deg/reg}}}{k_B T} \right] \quad (6)$$

where C is a constant, k_B is the Boltzmann constant, T is the temperature and $E_{\text{deg/reg}}$ are the degradation and regeneration activation energies, respectively. According to our knowledge, this is the first systematic study of E_{a} for LeTID along the brick. The $E_{\text{a,deg}}$ and $E_{\text{a,reg}}$ of the wafers at the same brick height show no difference within the error bars. As previously reported, similarity between $E_{\text{a,deg}}$ and $E_{\text{a,reg}}$ is an indication of a similar process involved during the degradation and regeneration processes [12,27], possibly due to the effect of hydrogen. This result indicates that the LeTID in the whole brick would have the same cause and might be mitigated in a similar manner. Besides, both $E_{\text{a,deg}}$ and $E_{\text{a,reg}}$ have a tendency of larger values towards the brick bottom. This is possibly related to the difference in dopant and dislocation concentrations.

5. Discussions

5.1. Activation energy E_a

Previous studies of Bredemeier et al. [31] proposed a two process defect model to simulate the whole degradation process, and the reported activation energy was 0.89 ± 0.04 eV and 0.94 ± 0.06 eV for the fast and slow degradation components respectively, at an illumination level of 0.5 kW/m^2 . Both E_a values are close to the values we extracted from the lower (5%–45%) brick. In another study, Liu et al. [23] reported $E_{\text{a,deg}} = (0.63 \pm 0.11)$ eV, $E_{\text{a,reg}} = (0.68 \pm 0.02)$ eV with 938 nm laser at 45 kW/m^2 for $1.7 \Omega \text{ cm}$ wafers, which are smaller than all the values we extracted in this work with resistivity ranging $0.82\text{--}1.33 \Omega \text{ cm}$. First, the difference in resistivity would not be the main reason since data in this study suggest a positive correlation between resistivity and E_a . Secondly, more dislocations near the brick top (Fig. 1) possibly provide additional routes for hydrogen diffusion thus lowering E_a . Nevertheless, the identical activation energy of degradation and regeneration has been confirmed in our study as well as several other reports for p-type mc-Si, which indicates the same root cause for the degradation and regeneration processes. We also notice that $E_{\text{a,deg}}$ is larger than $E_{\text{a,reg}}$ for cast-mono and Cz silicon wafers, which requires further investigations to clarify the difference.

5.2. A universal degradation method

In this work, the degradation and regeneration rates of wafers from different vertical locations in brick does not show much difference. This

Table 2

Summary of E_a values. T range means the temperature range used to extract E_a values.

Wafer type	Resistivity ($\Omega \text{ cm}$)	Condition	T range ($^\circ\text{C}$)	$E_{\text{a,deg}}$ (eV)	$E_{\text{a,reg}}$ (eV)	Ref.
p-mc	0.82	45 kW/m^2 laser	134–176	0.76 ± 0.09	0.78 ± 0.11	This work
	1.06			0.74 ± 0.08	0.77 ± 0.13	
	1.13			0.84 ± 0.07	0.92 ± 0.15	
	1.22			0.87 ± 0.10	0.90 ± 0.10	
	1.33			0.92 ± 0.09	0.92 ± 0.07	
	1.7			0.78 ± 0.05	0.70 ± 0.04	Liu, 2018 [23]
p-mc	1.7	14.6 kW/m^2 laser 30.5 kW/m^2 laser 44.9 kW/m^2 laser 60.1 kW/m^2 laser 74.5 kW/m^2 laser	100–300	0.64 ± 0.04	0.67 ± 0.02	Liu, 2018 [23]
				0.63 ± 0.11	0.68 ± 0.02	
				0.62 ± 0.07	0.72 ± 0.03	
				0.62 ± 0.09	0.78 ± 0.08	
				1.08 ± 0.05	1.11 ± 0.04	Vargas, 2019 [27]
				1.23 ± 0.16	1.34 ± 0.08	Vargas, 2018 [32]
p-cast mono ^a	2	7 kW/m^2 LED	150–250	0.65 ± 0.05	0.80 ± 0.04	Zhou, 2020 [33]
n-Cz	2	DA 0.02 kW/m^2 Halogen	140–175	0.76 ± 0.02	0.97 ± 0.05	Daniel, 2019 [15]
				0.70 ± 0.05	0.83 ± 0.04	

^a PERC cells are used in this work while all the rest are lifetime samples.

roughly agrees with the UNSW's result [18] (bottom wafers appear to degrade and regenerate slightly faster), while differs from Hanwha's work (bottom wafers degraded least and regenerated faster, whereas top degraded slowly) [19]. We notice that the injection level in our study (45 kW/m^2) is similar to UNSW's (34.6 kW/m^2) while much larger than the Hanwha's (V_{oc} mode, close to 1 kW/m^2). A higher illumination intensity corresponds to a larger carrier injection level, and therefore faster LeTID degradation rate, according to Refs. [34].

Fig. 7(a) compares the Δn of different wafer positions on initial IDLS curves at two illumination intensities. At 1 kW/m^2 , the Δn of the brick top wafers (95%-wafer, green solid line) corresponds to $\sim 5.7 \times 10^{14} \text{ cm}^{-3}$, while the Δn of the brick bottom wafers (5%-wafer, black solid line) is $\sim 1.4 \times 10^{15} \text{ cm}^{-3}$. The latter is 2.5 times of the former. At 45 kW/m^2 , which is beyond the range of our tester, Δn could be estimated from the curve trend. The Δn of the brick bottom wafers is about 1.5 times of that on the top. As a consequence, the carrier injection level of the brick top wafers is much closer to that at the bottom under 45 kW/m^2 illumination. In other words, the carrier injection level at 45 kW/m^2 is not so sensitive to the mc-Si bulk properties, such as the defects density, resistivity, and the metal and oxygen impurities.

Fig. 7(b) describes Δn evolution of the wafer close to the brick bottom (5%-wafer) during degradation. Compared to the initial state (black solid line), Δn of the degraded state after 14 s (green solid line) is reduced by $\sim 30\%$ at 1 kW/m^2 , while almost the same at 45 kW/m^2 . Therefore, r_{deg} and r_{reg} , which are dependent on Δn , can be treated as constant in Eq. (5) during the degradation and regeneration process in this study.

6. Conclusions

In this paper, we found that the low resistivity ($0.82\text{--}1.33 \Omega \text{ cm}$) multi-crystalline silicon wafers used for PERC mass production show

Appendix C. Supplementary data

Supplementary data to this article can be found online at <https://doi.org/10.1016/j.solmat.2020.110735>.

Appendix A

The relation between NDD and n/p.

According to the SRH recombination theory for p-type material [35,36], the SRH lifetime τ_{SRH} for a certain defect center has a linear relation with respect to the ratio of electron to hole concentrations n/p (Eq. (A1)).

$$\tau_n = \frac{1}{\alpha_n N} \left[1 + \frac{Qn_1}{p_0} + \frac{p_1}{p_0} + X \left(Q - \frac{Qn_1}{p_0} - \frac{p_1}{p_0} \right) \right] \quad (\text{A1})$$

$$Q = \frac{\alpha_n}{\alpha_p} \quad (\text{A2})$$

where X is the ratio of electron to hole concentrations n/p , τ_n is the minority carrier lifetime, Q is a parameter defined in Eq. (A2), α_n and α_p is the recombination center's capture coefficient for electron and hole respectively. N is the concentration of the defect, p_0 is the equilibrium hole concentration determined from the measured resistivity, n_1 and p_1 are the SRH carrier concentrations [37].

Under the assumption of mid-gap of the LeTID defect and $Q \sim 42$, we can simplify (A1) as:

$$\tau_n = \frac{1}{\alpha_n N} [1 + QX] \quad (\text{A3})$$

For the same defect, the α_n and Q are constant. Therefore, τ_n is proportional to N at the same X . The NDD values extracted at injection level of $0.1N_A$ reflect the LeTID defect density for wafers with different resistivity.

Appendix B

IDLS curves for the as-fired wafer of different brick height wafers at 159°C .

LeTID behavior similar to the previously reported results. Identical k values ~ 35 along the brick height are found. For the first time, the activation energy for degradation ($E_{a,deg}$) and ($E_{a,reg}$) regeneration along the brick are studied, which shows $E_{a,deg} = E_{a,reg}$ and a tendency of larger values towards the brick bottom. A laser accelerated degradation condition is examined, which could activate more than 90% of the LeTID defects in lifetime samples from the whole brick. We believe the laser accelerated degradation condition can be used as a fast LeTID monitoring tool for industrial production.

CRediT authorship contribution statement

Zheng Yao: Conceptualization, Methodology, Validation, Investigation, Writing - original draft. **Daqi Zhang:** Methodology, Software, Investigation, Writing - review & editing. **Jian Wu:** Writing - review & editing, Supervision. **Fangdan Jiang:** Resources, Project administration. **Guoqiang Xing:** Project administration. **Xiaodong Su:** Writing - review & editing, Project administration, Funding acquisition.

Declaration of competing interest

The authors declare that they have no known competing financial interests or personal relationships that could have appeared to influence the work reported in this paper.

Acknowledgements

This work was supported by the Key University Science Research Project of Jiangsu Province under Grant No.16KJA140002, and the Priority Academic Program Development of Jiangsu Higher Education Institutions (PAPD), and the Jiangsu Planned Projects for Postdoctoral Research Funds.

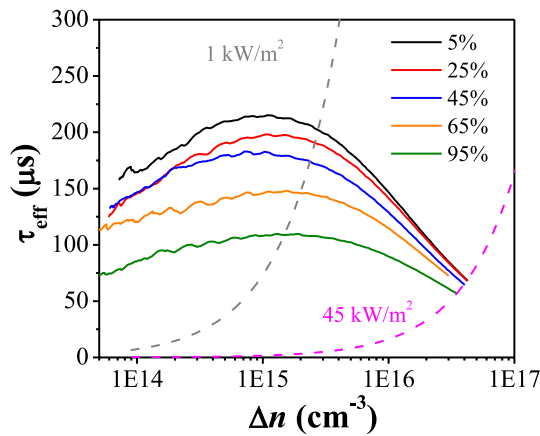


Fig. B. IDLS curves for the as-fired wafer of different brick height wafers at 159 °C.

Fig. B compares the Δn of different wafer positions on initial IDLS curves at two illumination intensities. At 1 kW/m^2 , the Δn of the brick top wafers (95%-wafer, green solid line) corresponds to $\sim 1.5 \times 10^{15} \text{ cm}^{-3}$, while the Δn of the brick bottom wafers (5%-wafer, black solid line) is $\sim 2.7 \times 10^{15} \text{ cm}^{-3}$. The latter is 1.8 times of the former. At 45 kW/m^2 , the Δn of the brick top wafers (95%-wafer, green solid line) corresponds to $\sim 3.4 \times 10^{16} \text{ cm}^{-3}$, while the Δn of the brick bottom wafers (5%-wafer, black solid line) is $\sim 4.2 \times 10^{16} \text{ cm}^{-3}$. The Δn of the brick bottom wafers is about 1.2 times of that on the top.

References

- [1] T. Dullweber, J. Schmidt, Industrial silicon solar cells applying the passivated emitter and rear cell (PERC) concept—a review, *IEEE J. Photovoltaics* 6 (2016) 1366–1381.
- [2] B.F. Kersten, P. Engelhart, H. Ploigt, A. Stekolnikov, T. Lindner, M.B.F. Stenzel, A. Szpath, K. Petter, J. Heitmann, J.W. Müller, A New Mc-Si Degradation Effect Called LeTID, *Photovoltaic Specialist Conference IEEE*, 2015.
- [3] J.H.K. Nakayashiki, A.E. Morishige, T.A. Li, D.B. Needleman, T.B. Mallory, A. Jensen, Engineering solutions and root-cause analysis for light-induced degradation in p-type multicrystalline silicon PERC modules, *IEEE J. Photovoltaics* 6 (2016) 860–868.
- [4] B.J. Hallam, P.G. Hamer, S.R. Wenham, M.D. Abbott, A. Sugianto, A.M. Wenham, C.E. Chan, G. Xu, J. Kraiem, J. Degou lange, R. Einhaus, Advanced bulk defect passivation for silicon solar cells, *IEEE J. Photovoltaics* 4 (2014) 88–95.
- [5] M. Padmanabhan, K. Jhaveri, R. Sharma, P.K. Basu, S. Raj, J. Wong, J. Li, Light-induced degradation and regeneration of multicrystalline silicon Al-BSF and PERC solar cells, *Phys. Status Solidi Rapid Res. Lett.* 10 (2016) 874–881.
- [6] C. Vargas, K. Kim, G. Coletti, D. Payne, C. Chan, S. Wenham, Z. Hameiri, Carrier-induced degradation in multicrystalline silicon: dependence on the silicon nitride passivation layer and hydrogen released during firing, *IEEE J. Photovoltaics* 8 (2018) 413–420.
- [7] D. Chen, M. Kim, B.V. Stefani, B.J. Hallam, M.D. Abbott, C.E. Chan, R. Chen, D.N. R. Payne, N. Nampalli, A. Ciesla, T.H. Fung, K. Kim, S.R. Wenham, Evidence of an identical firing-activated carrier-induced defect in monocrystalline and multicrystalline silicon, *Sol. Energy Mater. Sol. Cell.* 172 (2017) 293–300.
- [8] T. Nieuwelt, M. Selinger, N.E. Grant, W. Kwapił, J.D. Murphy, M.C. Schubert, Light-induced activation and deactivation of bulk defects in boron-doped float-zone silicon, *J. Appl. Phys.* 121 (2017) 185702.
- [9] H.C. Sio, H. Wang, Q. Wang, C. Sun, W. Chen, H. Jin, D. Macdonald, Light and elevated temperature induced degradation in p-type and n-type cast-grown multicrystalline and mono-like silicon, *Sol. Energy Mater. Sol. Cell.* 182 (2018) 98–104.
- [10] R. Eberle, W. Kwapił, F. Schindler, M.C. Schubert, S.W. Glunz, Impact of the firing temperature profile on light induced degradation of multicrystalline silicon, *Phys. Status Solidi Rapid Res. Lett.* 10 (2016) 861–865.
- [11] C. Chan, P. Hamer, G. Bourret-Sicotte, R. Chen, A. Ciesla, B. Hallam, D. Payne, R. Bonilla, S. Wenham, Instability of increased contact resistance in silicon solar cells following post-firing thermal processes, *Solar RRL* 1 (2017) 1700129.
- [12] C. Chan, T.H. Fung, M. Abbott, D. Payne, A. Wenham, B. Hallam, R. Chen, S. Wenham, Modulation of carrier-induced defect kinetics in multi-crystalline silicon PERC cells through dark annealing, *Solar RRL* 1 (2017) 1600028.
- [13] S. Liu, D. Payne, C. Vargas Castrillon, D. Chen, M. Kim, C. Sen, U. Varshney, Z. Hameiri, C. Chan, M. Abbott, S. Wenham, Impact of dark annealing on the kinetics of light- and elevated-temperature-induced degradation, *IEEE J. Photovoltaics* 8 (2018) 1494–1502.
- [14] T.H. Fung, M. Kim, D. Chen, C.E. Chan, B.J. Hallam, R. Chen, D.N.R. Payne, A. Ciesla, S.R. Wenham, M.D. Abbott, A four-state kinetic model for the carrier-induced degradation in multicrystalline silicon: introducing the reservoir state, *Sol. Energy Mater. Sol. Cell.* 184 (2018) 48–56.
- [15] D. Chen, P. Hamer, M. Kim, C. Chan, A. Ciesla nee Wenham, F. Rougier, Y. Zhang, M. Abbott, B. Hallam, Hydrogen-induced degradation: explaining the mechanism behind light- and elevated temperature-induced degradation in n- and p-type silicon, *Sol. Energy Mater. Sol. Cell.* 207 (2020) 110353.
- [16] D. Macdonald, A. Cuevas, A. Kinomura, Y. Nakano, L.J. Geerligs, Transition-metal profiles in a multicrystalline silicon ingot, *J. Appl. Phys.* 97 (2005), 033523.
- [17] G. Stokkan, Y. Hu, Ø. Mjos, M.J.S.E.M. Juel, S. Cells, Study of evolution of dislocation clusters in high performance multicrystalline silicon 130 (2014) 679–685.
- [18] D. Chung, B. Mitchell, P.P. Altermatt, T. Trupke, M. Abbott, Effect of wafer position in ingot on the light and elevated temperature induced degradation (LeTID) of multicrystalline silicon, in: Conference: 2018 IEEE 7th World Conference on Photovoltaic Energy Conversion, 2018, pp. 303–308.
- [19] F. Kersten, P. Engelhart, H.C. Ploigt, F. Stenzel, J.W. Müller, A new light induced volume degradation effect of mc-Si solar cells and modules. 31st European Photovoltaic Solar Energy Conference & Exhibition, 2015, pp. 1822–1826.
- [20] D.N.R. Payne, C.E. Chan, B.J. Hallam, B. Hoex, M.D. Abbott, S.R. Wenham, D. M. Bagnall, Rapid passivation of carrier-induced defects in p-type multi-crystalline silicon, *Sol. Energy Mater. Sol. Cell.* 158 (2016) 102–106.
- [21] D.N.R. Payne, C.E. Chan, B.J. Hallam, B. Hoex, M.D. Abbott, S.R. Wenham, D. M. Bagnall, Acceleration and mitigation of carrier-induced degradation in p-type multi-crystalline silicon, *Phys. Status Solidi Rapid Res. Lett.* 10 (2016) 237–241.
- [22] Catherine E. Chan, D.N.R. Payne, Brett J. Hallam, Malcolm D. Abbott, Tsun H. Fung, Alison M. Wenham, Budi S. Tjahjono, Stuart R. Wenham, Rapid stabilization of high-performance multicrystalline P-type silicon PERC cells, *IEEE J. Photovoltaics* (2016) 6.
- [23] S. Liu, C. Chan, D. Chen, M. Kim, C. Sen, U. Varshney, B. Hallam, M. Abbott, S. Wenham, D. Payne, Investigation of temperature and illumination dependencies of carrier-induced degradation in p-type multi-crystalline silicon, *AIP Conf. Proc.* 1999 (2018) 130014.
- [24] T.H. Fung, M. Kim, D. Chen, A. Samadi, C.E. Chan, B.J. Hallam, S. Wenham, M. Abbott, Influence of bound hydrogen states on carrier-induced degradation in multi-crystalline silicon, *AIP Conf. Proc.* 1999 (2018) 130004.
- [25] N. Nampalli, T.H. Fung, S. Wenham, B. Hallam, M. Abbott, Statistical analysis of recombination properties of the boron-oxygen defect in p-type Czochralski silicon, *Front. Energy* 11 (2016) 4–22.
- [26] B. Hallam, M. Abbott, N. Nampalli, P. Hamer, S. Wenham, Influence of the formation- and passivation rate of boron-oxygen defects for mitigating carrier-induced degradation in silicon within a hydrogen-based model, *J. Appl. Phys.* 119 (2016), 065701.
- [27] C. Vargas, G. Coletti, C. Chan, D. Payne, Z. Hameiri, On the impact of dark annealing and room temperature illumination on p-type multicrystalline silicon wafers, *Sol. Energy Mater. Sol. Cell.* 189 (2019) 166–174.
- [28] M.A. Jensen, A.E. Morishige, J. Hofstetter, D.B. Needleman, T. Buonassisi, Evolution of LeTID defects in p-type multicrystalline silicon during degradation and regeneration, *IEEE J. Photovoltaics* 7 (2017) 980–987.
- [29] A. Morishige, M. Jensen, D. Berney Needleman, K. Nakayashiki, J. Hofstetter, T.-T. Li, T. Buonassisi, Lifetime spectroscopy investigation of light-induced degradation in p-type multicrystalline silicon PERC, *IEEE J. Photovoltaics* (2017) 1–7.
- [30] Arrhenius equation, in: J.W. Gooch (Ed.), *Encyclopedic Dictionary of Polymers*, Springer New York, New York, NY, 2007, pp. 66–67.

- [31] D. Bredemeier, D. Walter, J. Schmidt, Light-induced lifetime degradation in high-performance multicrystalline silicon: detailed kinetics of the defect activation, *Sol. Energy Mater. Sol. Cell.* 173 (2017) 2–5.
- [32] C. Vargas, S. Nie, D. Chen, C. Chan, B. Hallam, G. Coletti, Z. Hameiri, Degradation and recovery of n-type multi-crystalline silicon under illuminated and dark annealing conditions at moderate temperatures, *IEEE Journal of Photovoltaics* 9 (2019) 355–363.
- [33] C. Zhou, F. Ji, S. Cheng, J. Zhu, W. Wang, D. Hu, Light and elevated temperature induced degradation in B–Ga co-doped cast mono Si PERC solar cells, *Sol. Energy Mater. Sol. Cell.* 211 (2020) 110508.
- [34] W. Kwapisil, T. Niewelt, M.C. Schubert, Kinetics of carrier-induced degradation at elevated temperature in multicrystalline silicon solar cells, *Sol. Energy Mater. Sol. Cell.* 173 (2017) 80–84.
- [35] R.N. Hall, Electron-Hole Recombination in Germanium 87 (1952) 221–229.
- [36] W. Shockley, W.T. Read, Statistics of the recombinations of holes and electrons, *Phys. Rev.* 87 (1952) 835–842.
- [37] J.D. Murphy, K. Bothe, R. Krain, V.V. Voronkov, R.J. Falster, Parameterisation of injection-dependent lifetime measurements in semiconductors in terms of Shockley-Read-Hall statistics: an application to oxide precipitates in silicon, *J. Appl. Phys.* 111 (2012) 113709.